# FoT25 2003 - 2005
# Propulsion Integration
# Final Report

MARLENE JOHANSSON (EDITOR)

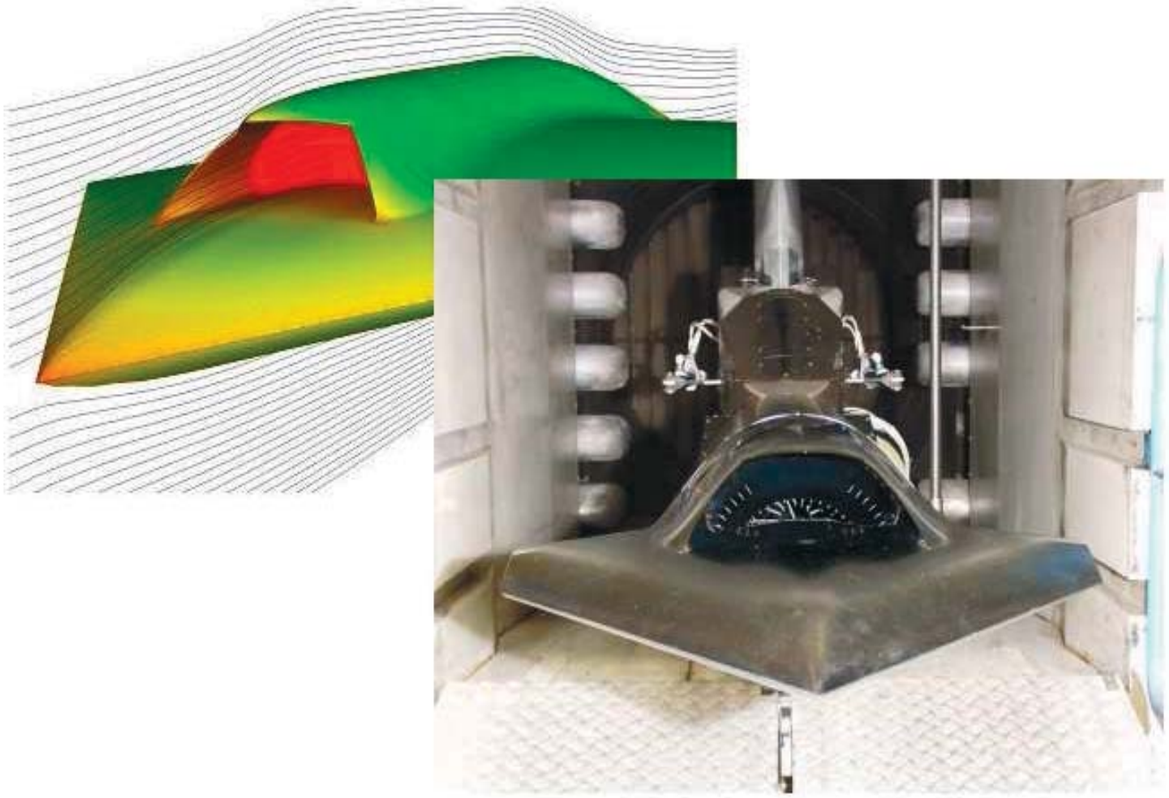

FOI is an assignment-based authority under the Ministry of Defence. The core activities are research, method and technology development, as well as studies for the use of defence and security. The organization employs around 1350 people of whom around 950 are researchers. This makes FOI the largest research institute in Sweden. FOI provides its customers with leading expertise in a large number of fields such as security-policy studies and analyses in defence and security, assessment of different types of threats, systems for control and management of crises, protection against and management of hazardous substances, IT-security an the potential of new sensors.

FOI
Defence Research Agency
Systems Technology
SE-164 90 Stockholm

Phone: +46 8 555 030 00
Fax: +46 8 555 031 00

www.foi.se

FOI-R--2017--SE
ISSN 1650-1942

User report
June 2006

**Systems Technology**

Marlene Johansson (editor)

# FoT25 2003-2005 Propulsion Integration Final Report

FOI-R--2017--SE User report
ISSN-1650-1942 June 2006

**Systems Technology**

| | | |
|---|---|---|
| **Issuing organisation**<br>FOI – Swedish Defence Research Agency<br>Systems Technology<br>SE-164 90 STOCKHOLM | **Report number, ISRN**<br>FOI-R--2017--SE | **Report type**<br>User report |
| | **Research area code**<br>Strike and Protection | |
| | **Month year**<br>June 2006 | **Project no.**<br>E61101 |
| | **Sub area code**<br>55. Air Vehicle Technologies | |
| | **Sub area code 2** | |
| **Author/s (editor/s)**<br>Marlene Johansson (editor) | **Project manager**<br>Marlene Johansson | |
| | **Approved by**<br>Monica Dahlén<br>Head, Systems Technology | |
| | **Sponsoring agency**<br>Swedish Defence Materiel Administration | |
| | **Scientifically and technically responsible**<br>Torsten Berglind | |
| **Report title**<br>FoT25 2003-2005: Propulsion Integration - Final Report | | |



**Abstract**

This report summarizes the work done in the FoT25-project ”Propulsion Integration”. A propulsion system for an UAV has been designed and analyzed, where the main focus as been the inlet. Analysis has been carried out with CFD calculations, wind tunnel testing, calculation of fluid-structure interactions and stealth properties.



**Keywords**

Propulsion integration, aerodynamics, structures, IR, RCS, CFD, wind tunnel, vortex generator

| | |
|---|---|
| **Further bibliographic information** | **Language** English |
| **ISSN** ISSN-1650-1942 | **Pages** 40 p. |
| | **Price acc. to pricelist** |

| | | |
|---|---|---|
| **Utgivare**<br>FOI – Totalförsvarets forskningsinstitut<br>Systemteknik<br>164 90 STOCKHOLM | **Rapportnummer, ISRN**<br>FOI-R--2017--SE | **Klassificering**<br>Användarrapport |
| | **Forskningsområde**<br>Bekämpning och skydd | |
| | **Månad år**<br>Juni 2006 | **Projektnummer**<br>E61101 |
| | **Delområde**<br>55. Flygfarkostteknik | |
| | **Delområde 2** | |
| **Författare/redaktör**<br>Marlene Johansson (editor) | **Projektledare**<br>Marlene Johansson | |
| | **Godkänd av**<br>Monica Dahlén<br>Chef, Systemteknik | |
| | **Uppdragsgivare/kundbeteckning**<br>FMV | |
| | **Tekniskt och/eller vetenskapligt ansvarig**<br>Torsten Berglind | |
| **Rapportens titel**<br>FoT25 2003-2005: Framdrivningsintegration - Slutrapport | | |



**Sammanfattning**

Den här rapporten sammafattar arbetet inom FoT25-projektet ”Framdrivningsintegration”. Ett framdrivningssystem för en UAV har designats och analyserats, där huvudfokus har varit luftintaget. Framdrivningssystemet har analyserats med CFD-beräkningar, vindtunnelprov, beräkningar av fluid-strukturinteraktion och signaturegenskaper.



| | |
|---|---|
| **Nyckelord**<br>Framdrivningsintegration, aerodynamik, struktur, IR, radar, CFD, vindtunnel, virvelgeneratorer | |
| **Övriga bibliografiska uppgifter** | **Språk** Engelska |
| **ISSN** ISSN-1650-1942 | **Antal sidor:** 40 s. |
| **Distribution enligt missiv** | **Pris: Enligt prislista** |

# Contents

# Nomenclature

| | |
|---|---|
| $\varepsilon$ | Emissivity |
| $\rho$ | Reflectivity |
| AIP | Aerodynamic Interface Plane |
| CFD | Computational Fluid Dynamics |
| $DC_{60}$ | Circumferential distortion descriptor for a 60° sector |
| dBsm | Decibel square meters |
| DES | Detached Eddy Simulation |
| Edge | CFD flow solver |
| EIKON | UAV concept |
| EM3D | RCS prediction tool |
| FE | Finite Element |
| FEM | Finite Element Method |
| HH | Horizontal transmit, Horizontal receive |
| $hp$ | Element length, Polynomial order |
| IR | Infra Red |
| LO | Low Observable |
| LCO | Limit Cycle Oscillation |
| M | Mach number |
| $\dot{m}$ | Mass flow |
| PEC | Perfect Electrical Conductor |
| PR | Pressure Recovery |
| RAM | Radar Absorbing Material |
| RANS | Reynolds Averaged Navier Stokes |
| RAS | Radar Absorbing Structure |
| RCS | Radar Cross Section |
| SIGGE | IR prediction tool |
| Stripe | FE-structural analysis system |
| TVC | Trust Vector Control |
| UAV | Unmanned Aerial Vehicle |
| UCAV | Unmanned Combat Aerial Vehicle |
| URAV | Unmanned Reconnaissance Aerial Vehicle |
| VG | Vortex Generator |
| VV | Vertical transmit, Vertical receive |

# 1 Introduction

This is the final report for the FoT25-project "Propulsion Integration" (Framdrivningsintegration), which has been running from 2003 to 2006.

The purpose of this project is to increase the competence at the Swedish defence authorities regarding the capability to evaluate and analyze propulsion concepts for UAV configurations. Evaluation of UCAV- or URAV-concepts includes detail analysis of critical parts. The propulsion system is such a critical part. Future military aircrafts will have shorter and more aggressive channels and mainly 2D outlets, which sets high requirements on the aerodynamic design.

The "Propulsion Integration" project has three different but complementing directions; to develop a general competence in the propulsion, to develop basic technology and methodology and through application connected to current industry project develop the capability to evaluate a given propulsion concept.

The general competence in the propulsion systems have been achieved by studying different trends in the development in propulsion. Alternative propulsion systems as been studied and a concept for an existing vehicle has been designed. This work is presented shortly in section 7 and in more detail in Refs. [1, 2].

The basic technology and methodology have included tools for modeling radarsignatures [3, 4, 5], IR-signatures [6, 7] and modeling of vortex generators [8, 9]. These tools have been used in the applications within the project.

The main part of the project has been to gain experience and knowledge in designing and analyzing compact, aggressive, low signature (stealth) inlet and outlet systems, primarily for UAV platforms. This has been done in collaboration with the industry[1] FoT25-project "TVC/LO Inlet and Outlet". The results gained from these projects will provide Sweden with a better ability in evaluating appropriate propulsion systems for both UAVs and manned aircrafts.

Figure 1.1: The external geometry, EIKON.

Within the projects, "Propulsion Integration" and "TVC/LO Inlet and Outlet", an inlet and an outlet system have been designed as well as a new

[1] Volvo Aero Corporation and Saab Aerosystems

type of engine concept to fulfill the requirements defined within the projects. Design and analysis of the inlet and the duct have been the main responsibilities of FOI. As external geometry, the EIKON geometry, designed in the FoT25-project "Design of a Low Signature UCAV" at FOI [10, 11], has been used as reference, see Figure 1.1 and the description in section 2. EIKON is designed to be a high subsonic, low altitude, low observable U(C)AV. The propulsion system has demands on aerodynamics, engine performance, structure dynamics and stealth; disciplines in the project included mainly through computational analysis, see sections 4, 5 and 6. The aerodynamic performance of the system has been verified through experiments, section 4.

The results from the project have been reported in several FOI reports and articles. The main results have been presented at national and international conferences. References to all reports, papers and conference contributions are presented in section 8.

# 2 External design and requirements

## 2.1 Eikon - the baseline design

The external geometry, EIKON, chosen for this project, was designed within the FoT25-project "Design of a Low Signature UCAV" at FOI [10, 11]. EIKON is designed to be a high subsonic, low altitude, low observable U(C)AV. It has a span width of 8 m, a total length of 8 m and a reference area of 32 $m^2$. Eikon has a take-off weight of 6000 kg. The reference data of Eikon is presented in Figure 2.1.

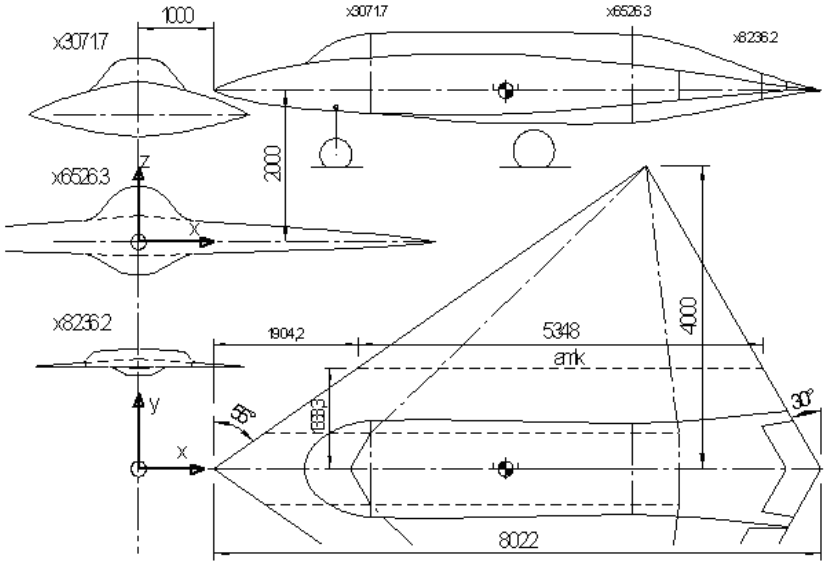


Figure 2.1: The reference data of EIKON.

Eikon shall be able to take-off and land within 800 m and has a range of 1000 km with cruise speed M=0.85 at height 11 km. The maximum speed should be M=0.95 at sea level.

Eikon has stealth requirements for radar and IR-signatures.

## 2.2 Requirements of the propulsion system

Within the "Propulsion Integration" project, the requirements are slightly relaxed compared to the requirements set in "Design of a Low Signature UCAV". The requirements are described in detail in Ref. [12].

### 2.2.1 General

The envelope is described by

**Angle of attack** -5° to 20 °

**Sideslip** -10° to 10 °

The aircraft should be able to take-off and start within 1800 m and has a range larger than 1500 km. The maximum speed should be M=0.85 at sea level.

The stealth requirements are also slightly relaxed compared to the project "Design of a Low Signature UCAV", see Ref. [12].

### 2.2.2 Engine

A new type of engine concept, Eikon_30, was designed by Volvo Aero [13]. Eikon_30 has a maximum normalized mass flow rate requirement of 62.5 kg/s including a 10% design margin. The actual flow demand at sea level, standard day with an estimated pressure recovery of 95% would be 59.4 kg/s. The AIP pressure distortion ($DC_{60}$) should be lower than 0.20 and the pressure recovery larger than 95%.

# 3 Experimental resources and software

FOI has advanced experimental resources in the form of wind tunnels and test rigs. With these assets, FOI is able to carry out testing and evaluation, at speeds ranging from subsonic to hypersonic. The most significant resource is the T1500 wind tunnel which gives FOI the possibility of testing at the high Reynolds numbers required for accurate simulation of flight conditions with continuous Mach number from M=0.2 to M=1.25 and at the fixed Mach numbers M=1.4 and M=1.7.

FOI has developed an advanced in-house flow solver Edge [14, 15], which has been used for all CFD calculations by FOI in this project. The Edge CFD code is based on an unstructured, dual mesh formulation and is capable of solving flow equations including Reynolds Averaged Navier Stokes (RANS) and Detached Eddy Simulation (DES) for complex geometries. Edge is open source software under license agreement used by aerospace industries, research institutes and universities.

Stripe [16, 17] is a high-performance 3D structural code developed by FOI. This *hp*-version type research code is a pure displacement solid continuum based approach for accurate and reliable numerical FE simulations of 3-dimensional time-harmonic linear viscoelasto-dynamic response problems in the low- and mid-frequency range. Stripe is used by FOI for a variety of advanced applications including simulation of fatigue and failure in aircraft structures.

The contribution to the overall RCS from cavities is predicted and analyzed most accurately using a FE-based method. The FE-code EM3D [3, 4, 5] has been used in this project. EM3D is developed by FOI together with the Institute for Computational Engineering and Sciences (ICES) in Texas, USA, and the Technical University of Cracow in Poland. EM3D is state-of-the-art in that it offers fully self-adaptive capabilities for discretization error control using the *hp*-version of the FEM. The *hp*-adaptive capability is optimal when it comes to resolving, for example, diffraction phenomena at irregular geometries and/or at RAM interfaces.

The simulation tool SIGGE [6, 7, 18], which has been developed at FOI, has been used for IR signature analysis. The SIGGE code is a 3D Ray Tracing code, which can handle a large number of specular reflections. The code can handle complex geometries and works with a number of commonly used commercial CFD formats.

# 4 Aerodynamics and design

## 4.1 Aerodynamics and design of the inlet

Several highly offset, single and double S-curved center line ducts have been designed and evaluated using CFD [19, 20], where configuration (c) in Figure 4.1, referred to as FOI-EIC-01, was chosen for further consideration since it was the higher challenge matching the objects of the project.

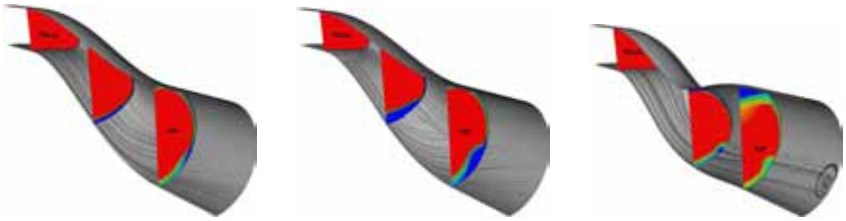

(a) (b) (c)

Figure 4.1: CFD calculations of two single- and one double bend inlet ducts. All ducts fit the EIKON configuration. Stream lines and total pressure are shown.

### 4.1.1 Analysis of inlet duct

The double S-curved center line duct FOI-EIC-01 has been evaluated in a rig test at FOI [21], Figure 4.2, and the experimental data has been compared to CFD calculations [19, 20]. The total pressure plot comparison between

Figure 4.2: Experimental setup of the duct FOI-EIC-01.

experimental measurements and CFD in Figure 4.3 indicate the same flow

features, a massive separation with low total pressure at the upper part and two smaller on each lower side, but the experimental setup failed to reach design mass flow target.

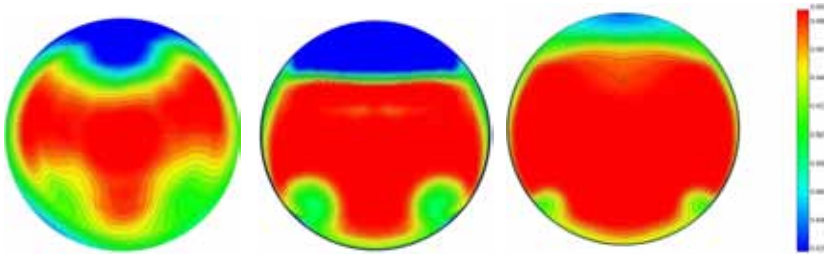

(a) Experiment (b) Model scale CFD (c) Full scale CFD

Figure 4.3: Experimental total pressure at AIP compared to corresponding CFD calculations for the duct FOI-EIC-01.

The experimental plot is at a lower mass flow rate, which due to experimental limitations was about 80% of the design mass flow target. Pressure recovery and $DC_{60}$ values are summarized in Table 4.1.

| | Experiment | Model scale CFD | Full scale CFD |
|---|---|---|---|
| $\dot{m}$ | 83% | 100% | 100% |
| PR | 0.937 | 0.941 | 0.978 |
| $DC_{60}$ | 0.556 | 0.598 | 0.284 |

Table 4.1: Mass flow, total pressure recovery and $DC_{60}$ for FOI-EIC-01, experiment and CFD.

In model scale, the recovery and DC60 predicted with CFD are very consistent with experimental data. However, this is comparing at two different mass flow conditions. Furthermore, the experimental values are taken at 50.4 mm downstream the actual AIP, where the measuring cell was located. The full scale CFD results shows better recovery and lower distortion indicating a Reynolds number effect.

Figure 4.4 shows the comparison of pressure recovery versus mass flow rate and throat Mach number. The full scale duct results are also shown for comparison. The Reynolds number, based on AIP diameter and throat velocity, is approximately $0.55{\cdot}10^6$ at 80% of design target in both experiment and model scale CFD. There is a major difference in recovery between the two CFD solutions. The full scale duct computations predict a pressure recovery 2-3% higher.

The experimental and computational values show the same trend in pressure recovery with increased mass flow rate, but the recovery is generally lower in the experiments. Comparing the recovery versus throat Mach number shows the same large differences. The throat Mach number was not directly measured in the experiments but is a function based on mass flow rate, area and reference total pressure. Based on these experimental Mach numbers, the flow does not seem to be choked in the throat since the highest value of Mach number is 0.55. It is not clear why the design mass flow target could not be reached but it is believed that the flow choked at some part in the setup behind the duct diffuser. The tests had to be completed in a hurry and no time was left for further investigations since the facility was permanently closed just after the tests were completed.

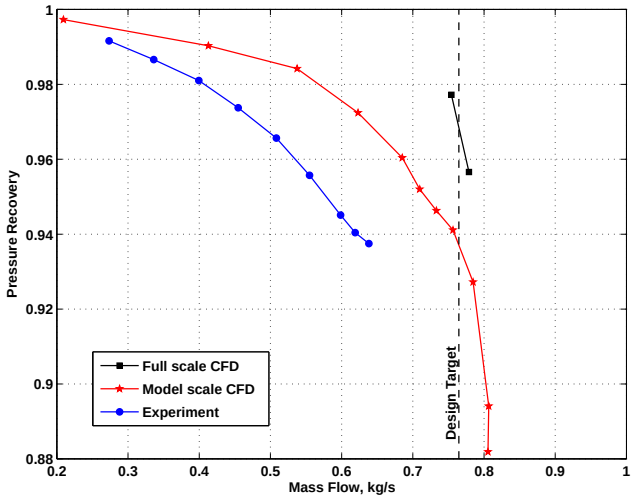


(a) Pressure recovery vs. mass flow

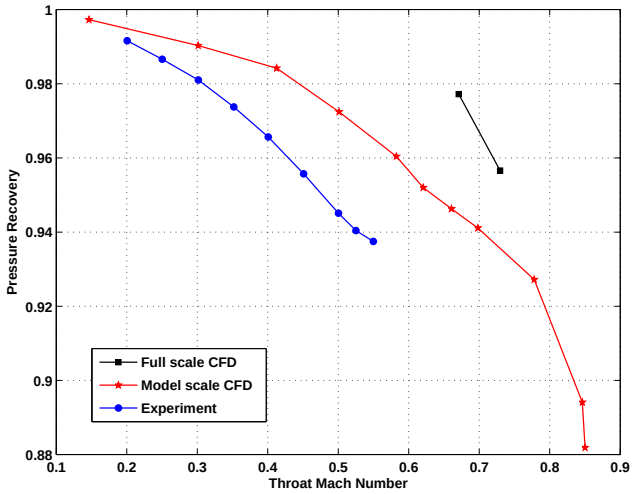


(b) Pressure recovery vs. throat Mach number

Figure 4.4: Experimental verification of the duct FOI-EIC-01.

The pressure recovery design target was set at 0.95 or better. This was achieved in the CFD solutions and almost in the experiment. But the distortion was far from the required $DC_{60}$ of 0.20. Thus, flow control is needed, see section 4.1.2 below.

The experiment and the CFD calculations are described in more detail in reference [19, 20, 22].

### 4.1.2 Flow control

The duct, FOI-EIC-01, has a very high value of the circumferential distortion exceeding given limit for maximum distortion. It is caused by flow separation in the duct accompanied by total pressure losses. In order to improve the inlet performance, flow control has been designed. Based on previous research and experiences at FOI, it was decided to employ micro-vortex generators flow control. The basic mechanism is to restructure the flow inside the inlet. This flow control studied for example in [23, 24] was extensively tested at FOI by using Edge and a vortex generator model [8]. The results published in [9]

suggest that there is a possibility to design a flow control without a need to run the time consuming optimization process by taking parameters of optimal vortex generator flow control settings, which are dependent mostly on location of separation and boundary layer thickness. Because of the complicated geometry, two flow control concepts were designed - one and two vortex generator row installation [25]. Figure 4.5 shows the izosurface of total pressure for arbitrary chosen value in the channel without and with flow control. Both VG installations eliminated flow separation which can be then seen immediately in the AIP plane with distribution of total pressure losses. The flow control was able to reduce flow distortion by a factor of almost 10 whilst improving total pressure recovery by approximately 1.5% in total scale. It should be noted, that since the vortex generators are modeled rather then meshed, no friction losses are taken to account during CFD analysis. This may lower the benefit in pressure recovery or even lead to increase in overall total pressure loss.

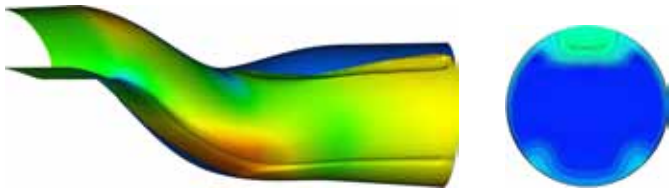

(a) **Baseline without vortex generators**

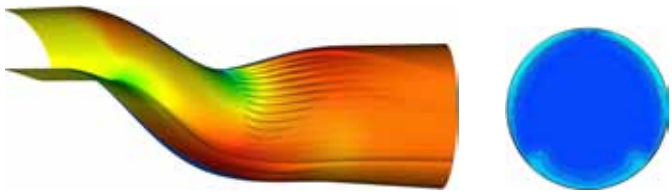

(c) **One row of vortex generators**

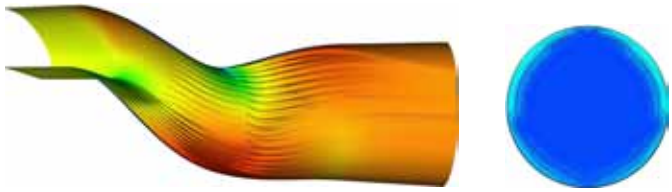

(e) **Two rows of vortex generators**

Figure 4.5: Flow control on the duct FOI-EIC-01. Total pressure on duct walls and at AIP.

### 4.1.3 Analysis of forebody, inlet and duct

A concept for the inlet, FOI-EIS-01, has been designed and analyzed using Edge [19, 20], see Figure 4.6. This inlet concept, including the forebody of EIKON, has been tested in the wind tunnel T1500 at FOI, Figure 4.7.

The experimental setup also includes the inlet duct FOI-EIC-01 and tests have been run with and without vortex generators, where the optimization with two rows described above has been used. Due to wind tunnel limitations, the experiments were not run at full scale Reynolds number. The highest Reynolds number corresponds to 55% of full scale Reynolds number. The Mach numbers were 0.6, 0.8 and 0.85. The angle of attack was varied from -5° to 20° in steps of 5° and the sideslip was varied from -10° to 5° in steps of 5°. Also the mass flow through the duct was varied.

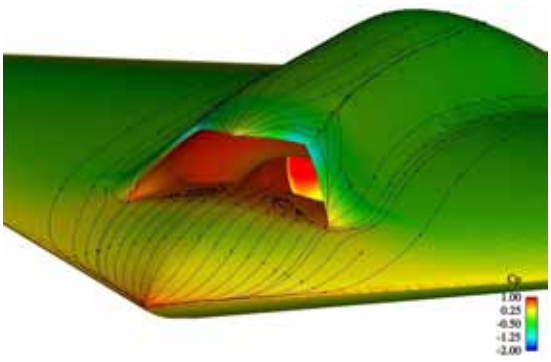

Figure 4.6: CFD calculation of the inlet FOI-EIS-01.

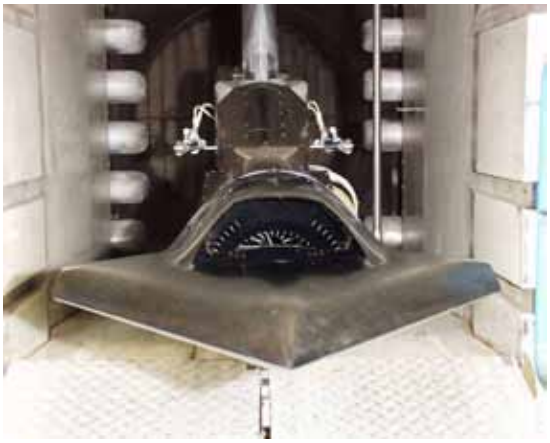

(a) Front view of the model.

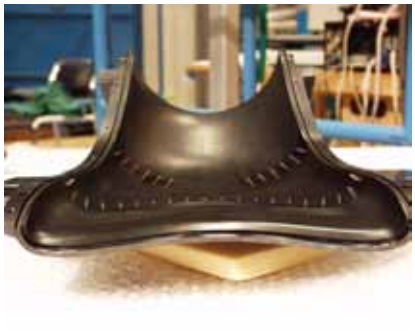

(b) Lower part of duct.

(c) Upper part of duct.

Figure 4.7: Pictures of the experimental setup FOI-EIS-01 in the wind tunnel T1500 including the duct, FOI-EIC-01, with two rows of vortex generators.

In this summary of the project, six cases are picked from the amount of experimental data as a representative examples. More details are found in the reports [19, 22, 25]. The chosen examples are for angle of attack $\alpha = 0°$ and sideslip angle $\beta = 0°$. Three cases without vortex generators at different Reynolds numbers are compared to three cases with vortex generators. Figure 4.8 shows the total pressures in AIP plane for the experiment. The six cases were repeated using CFD and duct geometry only. Figure 4.9 shows the calculated pressure recovery in AIP plane.

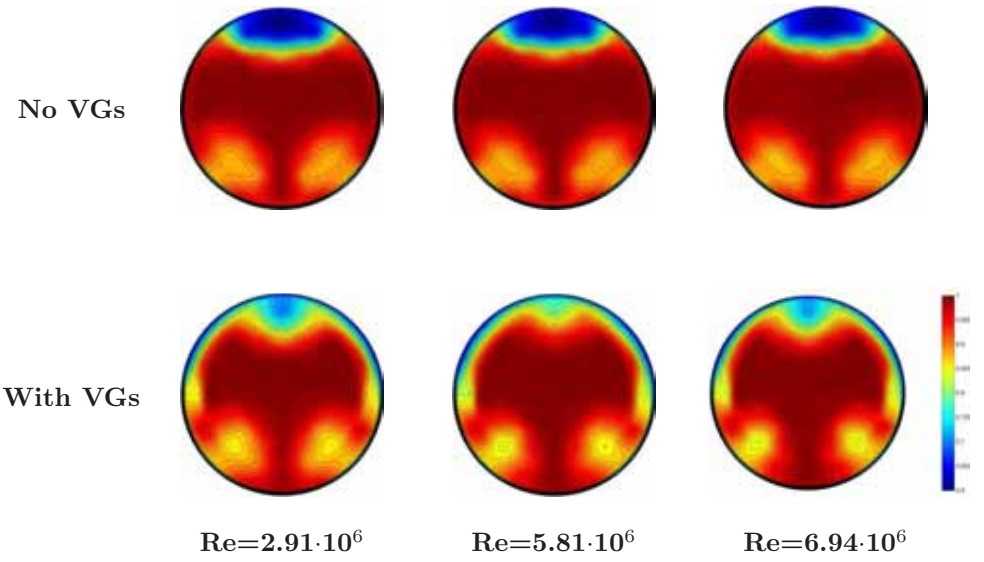


Figure 4.8: Total pressure at AIP without and with VGs, wind tunnel data.

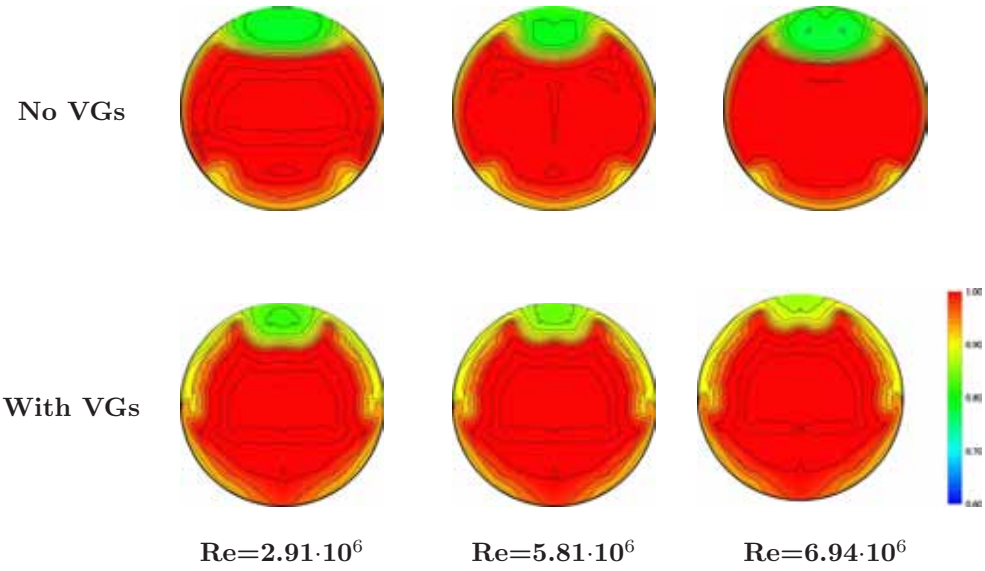


Figure 4.9: Total pressure at AIP without and with VGs, CFD data.

Compared to CFD data shown in Figure 4.9 there is a noticeable difference for the wind tunnel data in Figure 4.8. A separation on the lower side of the inlet, which is not prominent in calculations containing only the duct geometry, can immediately be marked. It is certainly an effect of the boundary layer from the model fore-body. This separation gives rise to typical spiral separation shown in Figure 4.10(a) with corresponding pattern in the AIP plane shown in Figure 4.10(b). Determining sector for the distortion, however, remains the upper part of AIP plane.

The separation on the upper side of the channel seems to be rather stable both in wind tunnel data and in the CFD calculations. The total pressure loss does not change between cases without and with vortex generators, see Table

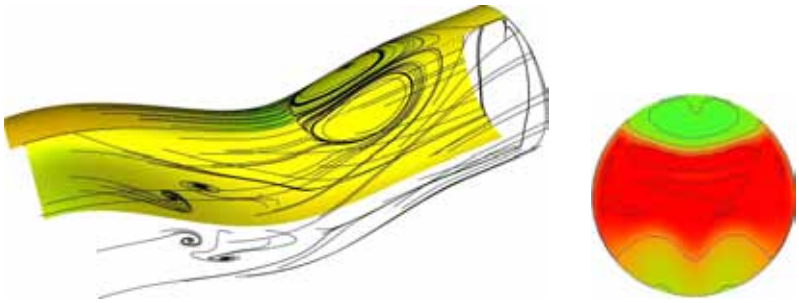

(a) (b)

Figure 4.10: Isosurface of total pressure including stream lines (a) and pressure recovery in the AIP plane (b), FOI-EIS-01 including forebody and inlet.

4.2. Comparing the CFD predicted improvement of total pressure recovery about $\Delta p_r \approx 1 \rightarrow 1.5\%$ with the actual losses due to viscous effects of vortex generators might be quite large reaching values on the order of percents. The CFD calculations show higher pressure recovery than experimental data. The reason for this is that in the CFD calculations the forebody is not included, as discussed above, and, thus, the losses in pressure are less. Still, the requirements for pressure recovery are achieved for both CFD and experimental data for Reynolds number higher than $5.8{\cdot}10^6$.

| | Experiment | | CFD | |
|---|---|---|---|---|
| *Re* | No VGs | VGs | No VGs | VGs |
| $3{\cdot}10^6$ | 0.947 | 0.946 | 0.962 | 0.967 |
| $5.8{\cdot}10^6$ | 0.951 | 0.954 | 0.967 | 0.972 |
| $7{\cdot}10^6$ | 0.951 | 0.953 | 0.965 | 0.975 |

Table 4.2: Pressure recovery for wind tunnel test and CFD

Table 4.3 shows the circumferential distortion in the AIP plane for wind tunnel test and CFD. Both CFD and experiments shows a reduction in distor-

| | Experiment | | CFD | |
|---|---|---|---|---|
| *Re* | No VGs | VGs | No VGs | VGs |
| $3{\cdot}10^6$ | 0.562 | 0.243 | 0.604 | 0.387 |
| $5.8{\cdot}10^6$ | 0.535 | 0.115 | 0.586 | 0.280 |
| $7{\cdot}10^6$ | 0.525 | 0.216 | 0.699 | 0.195 |

Table 4.3: $DC_{60}$ for wind tunnel test and CFD

tion when VGs are used. The level of reduction may depend on the boundary layer from the forebody. The thickness of the boundary layer on the inlet walls is a decisive factor for the effectiveness of flow control. The Reynolds number effect is not as clear. The CFD prediction with VGs shows a steady decreasing distortion with increasing Reynolds number whilst wind tunnel data show a minimum in the distortion around $5{\cdot}10^6$. It is known that CFD can have difficulties with distortion prediction. More serious is however the difference in trend in distortion with flow control. For the time being, the cause is not known. There are some issues which should be taken to account. The CFD uses inlet geometry without aircraft forebody which may have effect on the boundary layer. On the other side this effect would be mostly pronounced on

the lower side of the inlet and is visible as two domains of low pressure recovery at lower part of the AIP. The sharp minimum in distortion with flow control device is surprising and needs more study. But the general conclusion is that with vortex generators the distortion requirements are achieved for the two higher Reynolds numbers.

## 4.2 Final design of inlet and nozzle

Figure 4.11: EIKON, final design including inlet.

The final geometry of the propulsion system (inlet and nozzle) for EIKON is presented in Figure 4.12.

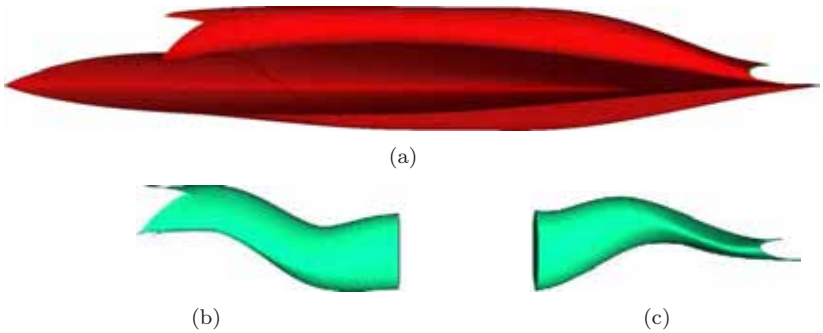


Figure 4.12: The UAV EIKON (a) seen from the side and the shapes of the (b) inlet and (c) nozzle.

The inlet system, FOI-EIS-01, was defined in section 4.1 and the outlet (Nozzle 6.0) has been design by Volvo Aero [26]. The complete design has been analyzed using CFD in section 4.3. The inlet duct and the nozzle has been analyzed using fluid-structured coupled CFD (section 5) and with advanced stealth prediction methods (section 6).

## 4.3 CFD analysis of complete design

The entire EIKON airframe, fuselage, inlet and outlet, was calculated at different flight conditions given by flight envelope which is shown in Figure 4.13. The entire flow was solved as inviscid, because it saves time for mesh generation and calculations. It enables to run a large number of cases in a short time but still obtain a number of parameters in the inlet such as data in the AIP plane.

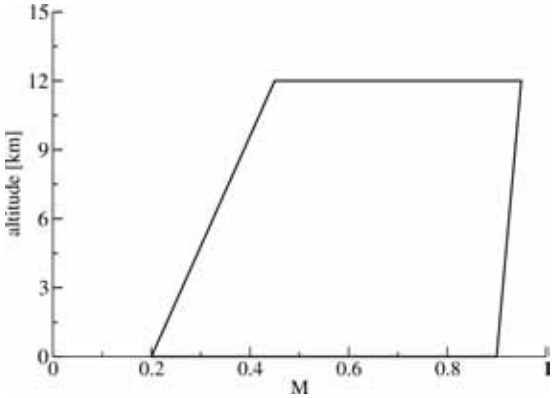


Figure 4.13: The EIKON envelope.

Since no engine characteristics for given flight conditions were available, the mass flow through the inlet was kept at its maximum required value or slightly lower than critical value. The aim of this study was to collect total pressure and total temperature in the inlet entrance, values of static pressure and average Mach number in the AIP plane and values of total pressure in the nozzle. For high altitude flights the result of analysis contains the value of critical mass flow at which the channel chokes. The channel choked at Mach number in the AIP exceeding values $M \approx 0.52 \rightarrow 0.53$ which is above limit $M \geq 0.5$ given in the specification. Figure 4.14 shows the importance of a such calculations. It shows the surface Mach numbers for aircraft flying at see level altitude at one flight Mach number with two different values of mass flow through the inlet.

As figure shows, the amount of flow through the propulsion unit determines the extent of spillover and its interaction with terminal shock wave. The values of total states in the inlet, mass flow through the inlet and average Mach number in the AIP were then used during analysis of the flow control at different flight conditions.

This is discussed further in Ref. [25].

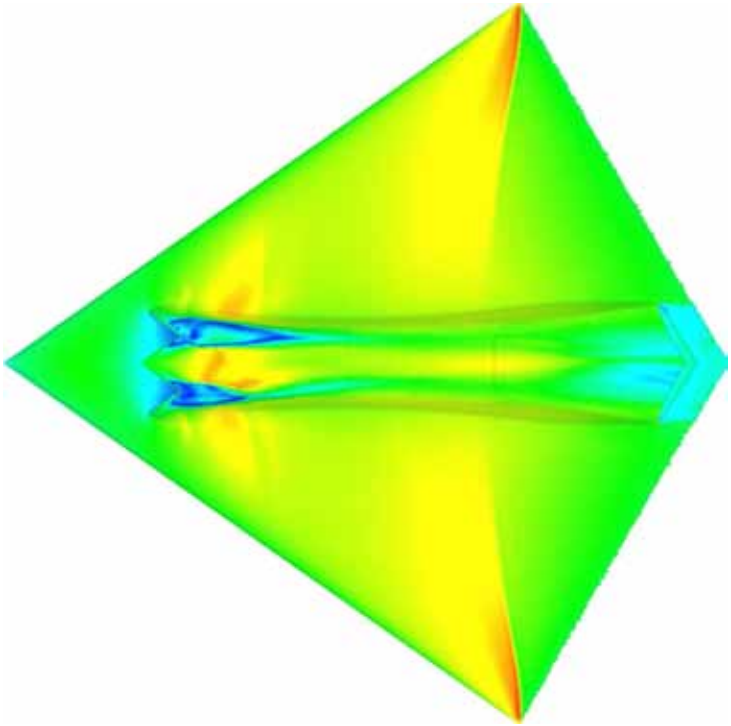

(a) $\dot{m} = 20\ kg/s$

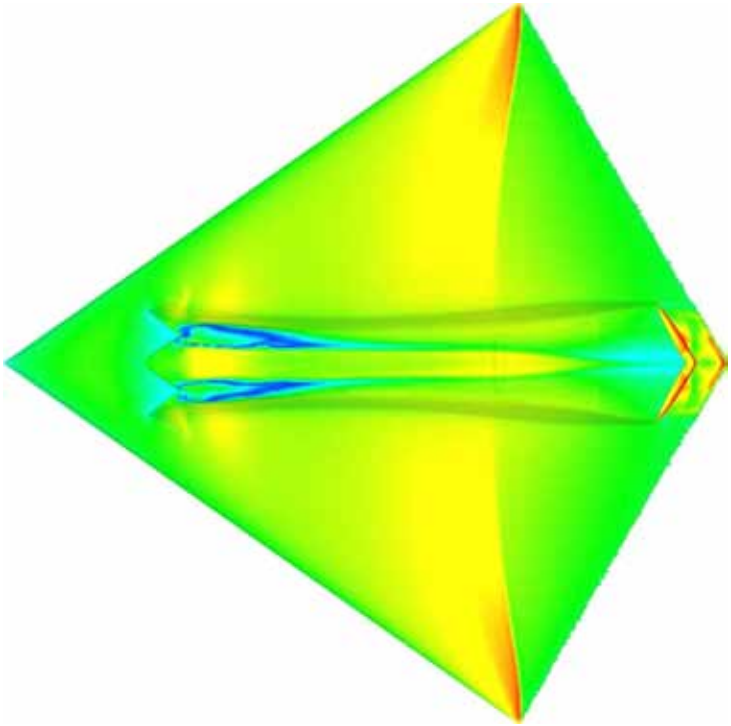

(b) $\dot{m} = 60\ kg/s$

Figure 4.14: Mach numbers on the surface of EIKON, two values of mass flow through propulsion unit, M$\infty$=0.85

# 5 Material and structure dynamics

## 5.1 Material

A literature review is given in Ref. [27], with focus on potentially useful materials and composite structures for aero applications. The fast development and potential use of composite materials for the inlet and outlet sections of a propulsion system, with high temperature capabilities and good signature properties are of high interest.

For the inlet, a structural dynamic analysis is done on three conceptual configurations. A standard metallic aluminum structure and two composite sandwich structures are studied. For the inlet the RCS (Radar Cross Section) was of high priority, in order to avoid detection by radar system.

For the outlet, a structural dynamic analysis is performed on two outlet configurations. A super-alloy structure and a sandwich structure. A brief discussion is made in Ref. [27] about new ceramic materials with low density, good strength properties, high temperature and corrosions resistants.

## 5.2 Fluid-structure interaction

It was anticipated from the outset of the project that the inlet duct and outlet nozzle used in EIKON could be sensitive to aeroelastic, fluid-structure interaction effects. The flow in these channels can be highly unsteady and due to the use of novel materials and structures, the dynamic behavior of these systems was largely unknown. Computational studies were carried out investigating the dynamics of selected duct structures including their interaction with the internal flow. This work on the inlet duct is described in detail in Ref. [28]. Results for the outlet will be published shortly [29]. Some results are presented here, including structures conforming to the inlet duct geometry FOI-EIC-01 and the outlet Nozzle 6.0, designed by Volvo Aero.

The tools used here comprise the FOI-developed codes Edge and Stripe, see section 3. The modal analysis was computed using Stripe. Coupled aeroelastic simulations in Edge are carried out with a simplified representation of the structure, based on normal modes of the free undamped structure. The implementation of this method in Edge is fully described in [30].

### 5.2.1 Inlet duct

Three structural models of the inlet duct, denoted I1-I3, have been analyzed. The FE-meshes for these models are shown in Figure 5.1 and the first three normal modes are shown in Figure 5.2. For all three models, the structure is clamped at the inlet and outlet planes. Structure I1 is a 4 mm thick single shell of Aluminum. Models I2 and I3 represent a special radar absorbing structure (RAS) with three outer layers of a fiber-reinforced composite enclosing a distance-material layer of polymer foam (total thickness 46 mm). Model I3 is identical to I2 apart from the addition of two stiffening rings. These three

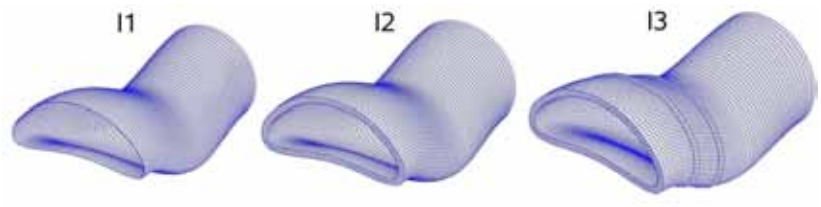


Figure 5.1: Meshes for the three FE-models of the inlet duct structure.

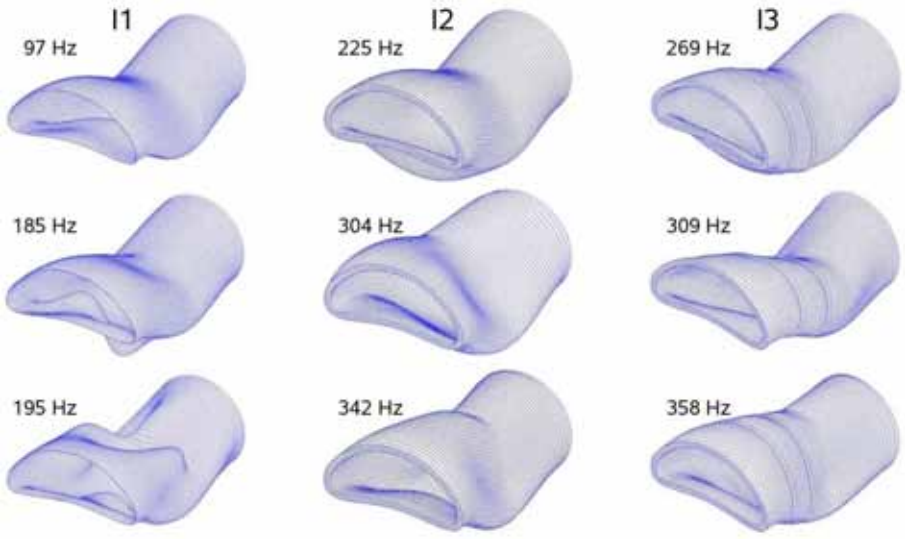


Figure 5.2: First three normal modes for structural models I1-I3.

structures have roughly similar masses: 42, 48 and 56 kg for I1-I3 respectively, but their dynamic properities are quite different. The resonant frequencies of the RAS structures are much higher than those of the simpler Aluminum shell.

Figures 5.3 and 5.4 show results from an Edge coupled CFD simulation, with inviscid, Euler flow, for the I1 structural model. Figure 5.3 shows the

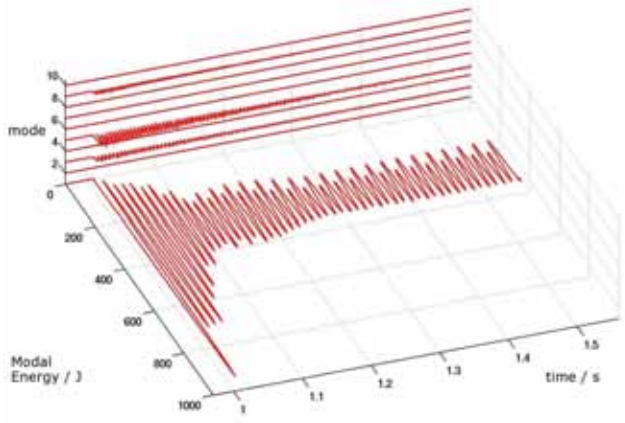


Figure 5.3: Structural energy, modal decomposition for structure I1.

time variation of the total energy of the structure, decomposed into its modal components (the first ten elastic modes). It can be seen that there is an initial

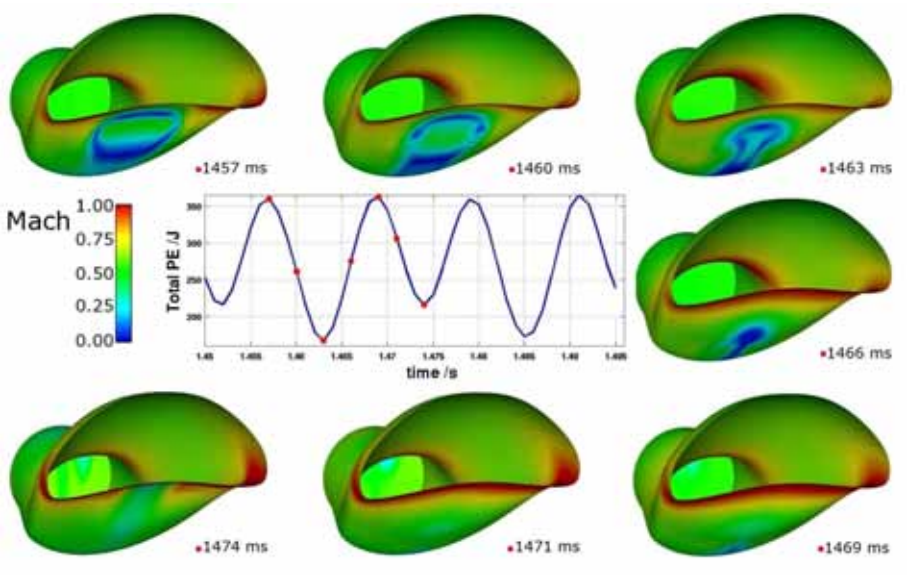


Figure 5.4: Mach-number field variation for a single LCO-cycle for structure I1.

transient response, in which modes 1, 3, 5 and 9 are active. However, when this transient decays away there remains a sustained, limit-cycle oscillation (LCO) which is dominated by the first structural mode. The second harmonic of the LCO, at 89.4Hz, is close to the "air off" frequency of mode 1. Figure 5.4 shows the time-evolution, of the surface geometry and Mach-number field, over one cycle of the LCO. The picture-samples are taken at the extrema of the total structural kinetic- and potential-energy. The amplitude of the surface movement is small, but produces a strong oscillation in the surface Mach number and large regions of low-speed flow propagating to the outflow plane.

Coupled simulations have been carried out for all three structural models at several operating conditions and the results are presented in detail in Ref. [28]. The results show that whilst fluid structure interaction effects are predicted for all three structures, the magnitude of the sustained oscillations in the more realistic RAS structures are very small and would be alleviated by internal structural damping.

The most important result of this work has been to demonstrate that with the existing CFD and FE tools we are able to predict LCO effects and to use this information to develop design solutions to eliminate them.

### 5.2.2 Outlet nozzle

Fluid-structure interaction simulations have also been carried out for Nozzle 6.0. The structure of the nozzle is represented by two FE-models, denoted O1 and O2, from which the first ten normal modes are extracted. For the coupled simulations, the resulting modal systems are modified by adding viscous damping. The surface meshes of the two FE-models are shown in Figure 5.5 together with the modeshapes of the first four modes.

The first structural model, O1, represents a single shell of uniform thickness of 3 mm, made of a temperature resistant super-alloy of type Inconel 706. The structure is clamped at the inlet plane but is otherwise unconstrained. The second model, O2, represents a more realistic RAS design with a bonded sandwich structure comprising outer plates of thickness 1 mm enclosing a distance material layer of thickness 7 mm. The exterior of the structure is augmented

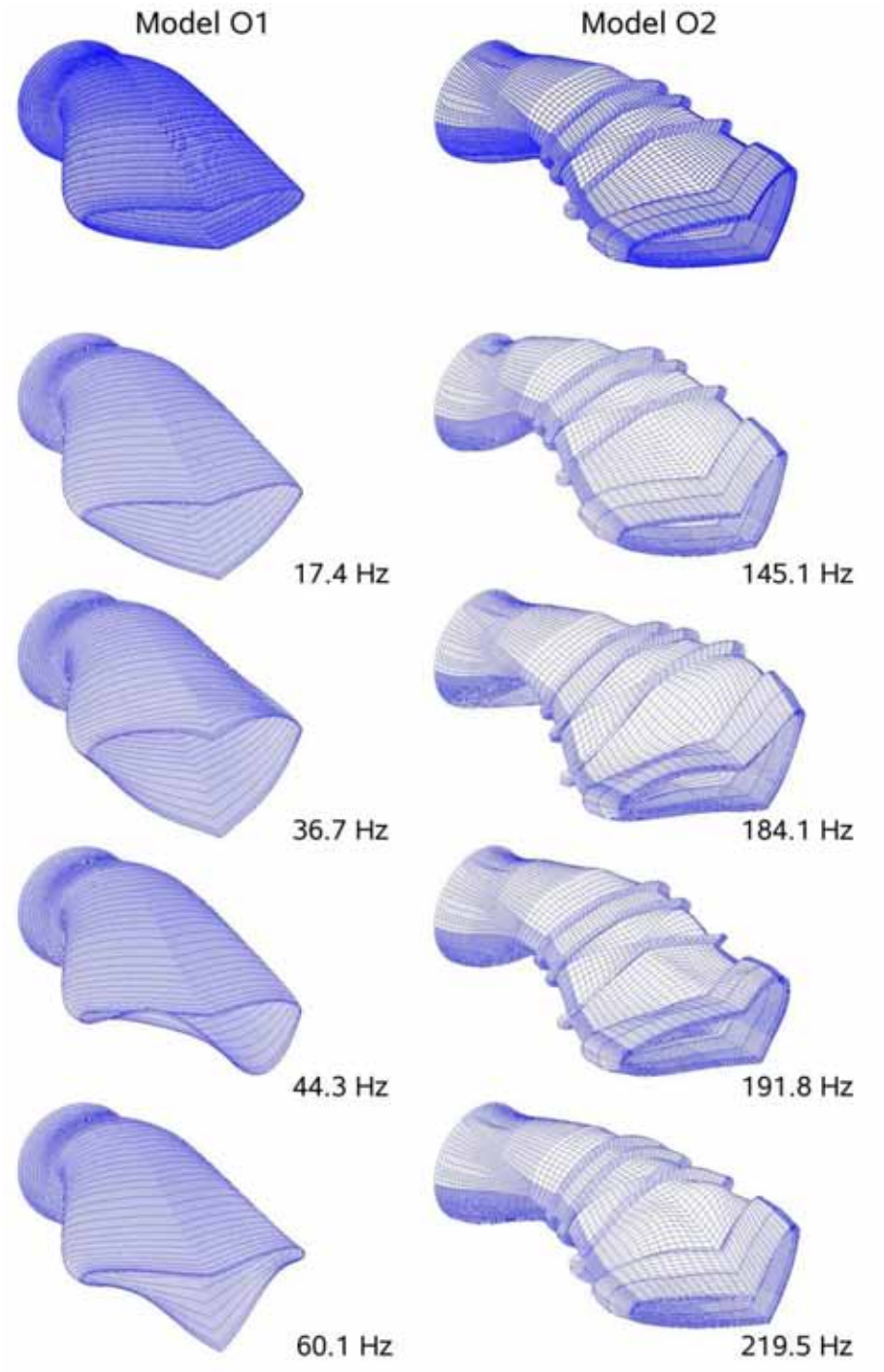


Figure 5.5: Surface meshes and first four modeshapes for structural models O1 and O2.

with six ring stiffeners and three small axial stiffeners under the lower surface of the outlet nozzle. The O2 structure is clamped at the inlet plane and an axial sliding boundary condition is set at five positions at the rear end of the structure.

Figure 5.6 shows surface pressure and Mach number distributions for steady-state solutions obtained with the rigid geometry and with the critically damped models O1 and O2.

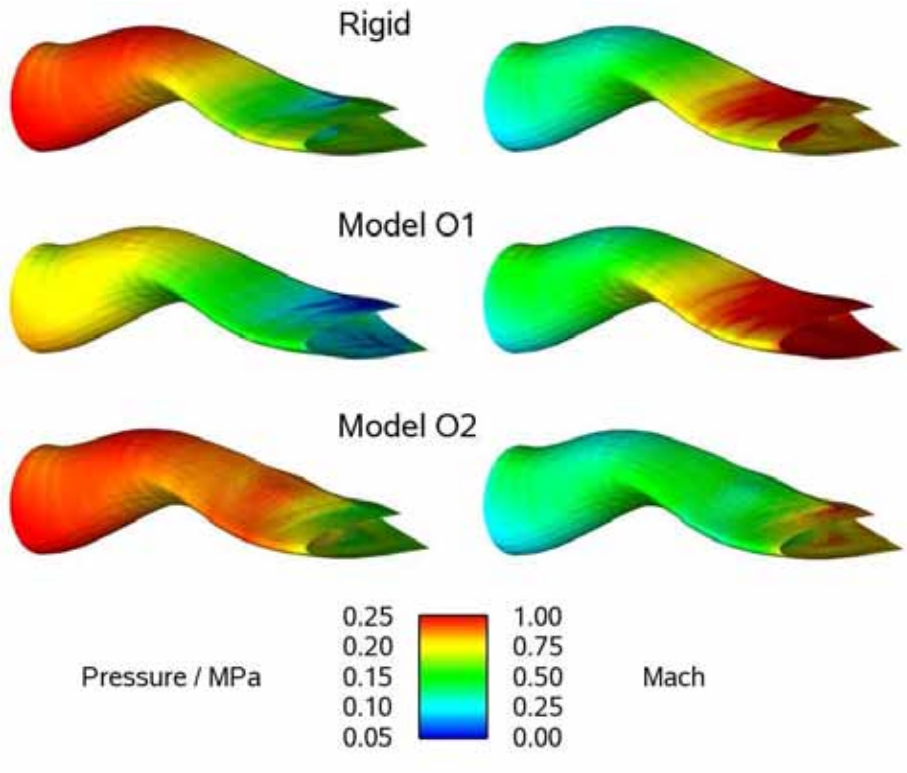


Figure 5.6: Steady-state surface pressure and Mach number distribution for the rigid geometry and the static equilibrium state of models O1 and O2.

The rigid-surface results show that the internal flow is choked, with a supersonic region extending about 0.5 m upstream of the outlet aperture. This results in very large internal pressures and structural loads. Futhermore, time-accurate solutions show that this flow is also highly unsteady, even with a completely rigid surface. Similar results are obtained for a wide range of inlet mass flows and temperatures. The results for the static-coupled solutions show clear evidence of structural interaction, with model O1 showing by far the largest effects. This structure is unstable with or without material damping.

With model O2, the large excess internal pressure results in balloon-like expansion of the structure about 0.2 m upstream the outlet. Near the outlet, however, the extra wall stiffening preserves the aperture shape. In contrast, the structure represented by model O1 is much more flexible and the effect of the internal pressure loading is to blow the outlet open. This effectively moves the nozzle aperture upstream, with the outer section of the nozzle acting as a shroud over the expanding supersonic flow. These results indicate that structure O1 is severely underdimensioned and that whilst structure O2 is more robust, additional stiffening is required to adequately contain the static pressure loading from the internal flow.

Dynamic coupled simulations were performed with the same structural

models, including the use of different levels of internal damping. Figure 5.7 shows results from these simulations in the form of a time history of the structural energy variation. The simulations were carried out using five levels of structural damping, defined by the parameter $\zeta$ (=1 for critical damping). For model O1, the dynamic coupled system is unstable for for all five damping cases. The motion is self-excited from unsteady flow and is predominantly in the outer edge of the nozzle. At the lower damping levels the response becomes so large that the solution terminates due to inverted cells in the CFD mesh. With heavier structural damping, a sustained LCO response is observed. However, any oscillation of this magnitude would, in practice, result in rapid structural failure. For the more robust structure represented by model O2, given a small initial excitation, the system also has an oscillatory reponse but it is stable even with zero structural damping. Further details of these calculations, including modal response spectra, are given in Ref. [30].

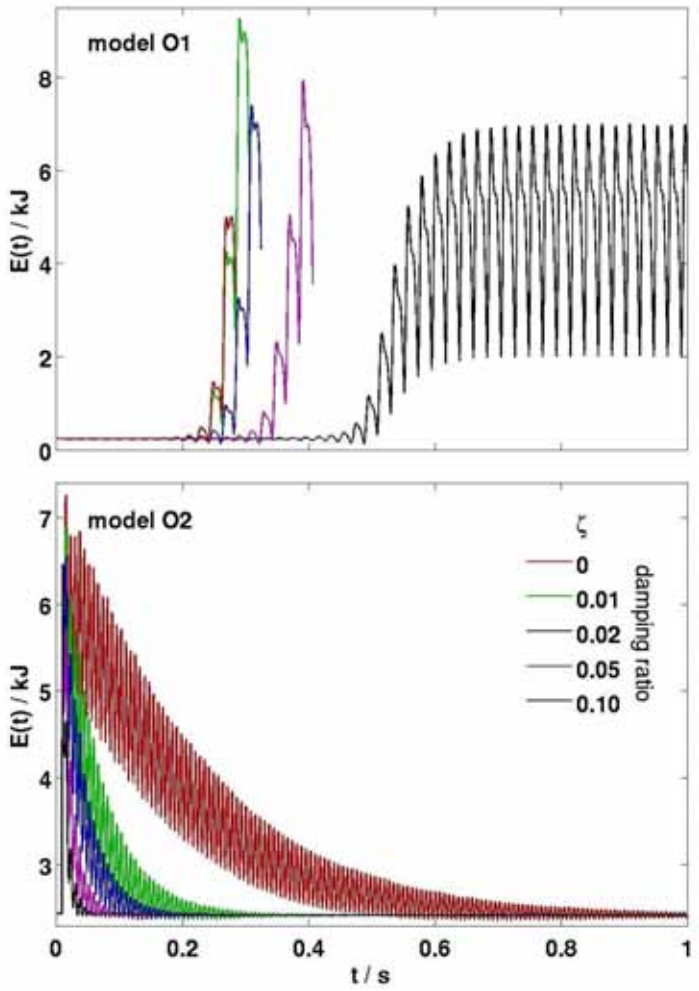


Figure 5.7: Structural energy timeseries for simulations with five different levels of structural damping.

The results obtained for these structural models show how a few relatively inexpensive simulations can be used to predict the flow-coupled dynamics. Static coupled simulations, which are especially cheap and quickly executed, can, in principle, be used at an early stage in the design process for dimensioning the nozzle and its supporting structure.

# 6 Stealth technology

## 6.1 Radar cross section

The radar cross section (RCS) of the inlet and the outlet has a large contribution to the RCS of the whole vehicle. Both the inlet duct and the outlet have been analyzed using the RCS code EM3D, see section 6.1.1 and section 6.1.2 below. The complete analysis is presented in Refs. [31, 32].

Within the Propulsion Integration project, the influence on the RCS from cavities by curvature, RAM and vortex generators have been studied [33]. The main conclusion regarding the effects from vortex generators is, as expected, that vortex generators smaller than the wavelength will not change the RCS. Vortex generators twice the size of the wavelenght are clearly visible.

### 6.1.1 RCS of inlet duct

For the double S-curved duct, FOI-EIC-01, the RCS has been calculated with and without RAM at 1 GHz with HH-polarization [31]. The duct without any RAM was modelled as a perfect electrical conductor (PEC) as a boundary condition. The RAM, consisting of two material layers, was constitutively modelled by material parameters in the FE-elements, i.e. the RAM layers were built up by finite elements having constitutive material properties given by conductivity, relative permittivity and relative permeability. Due to confidentiality, the level of the RCS can not be presented in Figure 6.1, where the result is shown. The RAM will reduce the RCS of the duct with roughly 2-3dBsm.

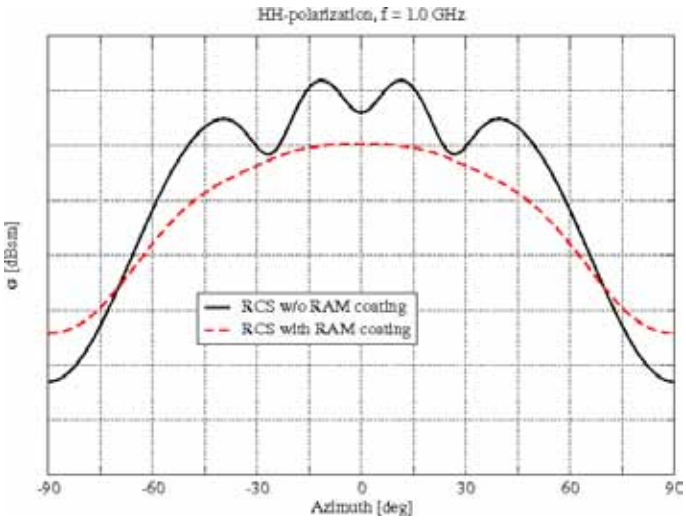


Figure 6.1: RCS of the inlet duct for a azimuth sweep at 0° degree elevation, HH-polarization.

### 6.1.2 RCS of outlet nozzle

The outlet nozzle, Nozzle 6.0, has been modelled with PEC boundary conditions, with the whole nozzle covered with RAM and with parts of the nozzle covered with RAM [32]. The calculations were performed with a frequency of 1 GHz, both with HH-polarization and VV-polarization. The RAM consisted of three material layers modelled in the same way as for the inlet duct, but with different material properties. The result for azimuth sweep at 0° elevation are presented in Figure 6.2.

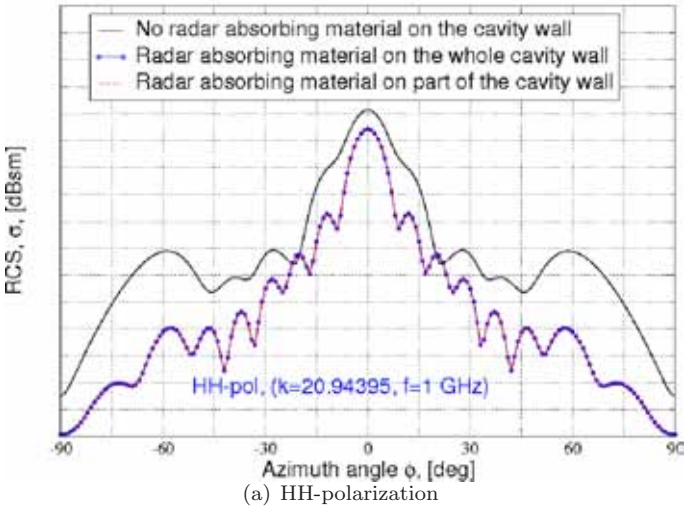


(a) HH-polarization

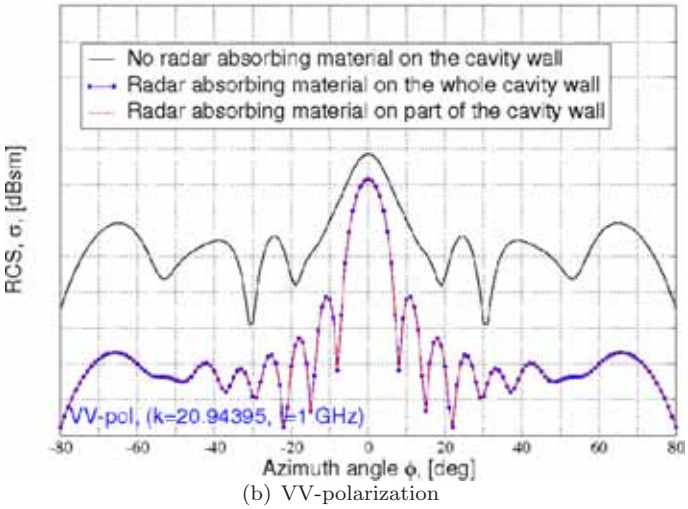


(b) VV-polarization

Figure 6.2: RCS of the nozzle for a azimuth sweep at 0° elevation.

The semi-covered cavity produces almost the same RCS as the whole cavity, which shows that to obtain this reduction in RCS it is sufficient with partial RAM coating.

## 6.2 IR signature

The main contribution to the IR signature comes from the exhaust flame and the hot parts in the outlet. Thus, in this project the IR calculations have been

focused on the outlet, using the IR prediction code SIGGE. To reduce the IR signature from the outlet, Nozzle 6.0 was used, see Figure 6.3.

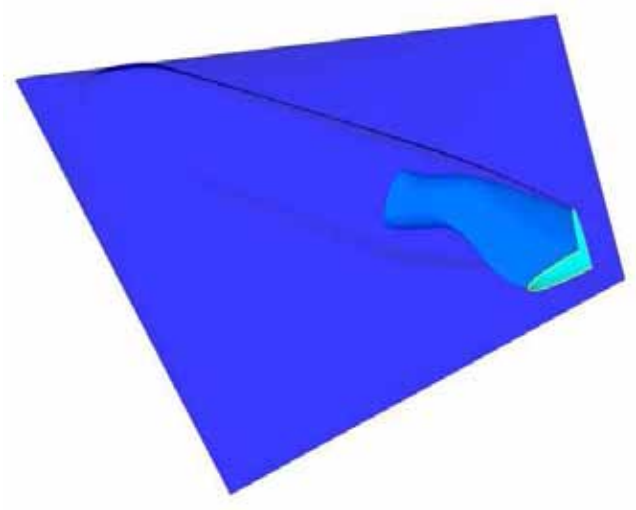

Figure 6.3: Geometry used for IR calculations, with the fuselage partly transparent to visualize the shape of the nozzle.

The aircraft was assumed to fly at a speed of M=0.85, at sea level (the design point). The IR calculations were preformed with 1000×1000 pixel and the emissivity was set to $\varepsilon$=0.7 and the reflectivity to $\rho$=0.3. The wave-number intervals were set to 830cm$^{-1}$-1250cm$^{-1}$ and 2000cm$^{-1}$-2800cm$^{-1}$, with a resolution of 5cm$^{-1}$. For the temperature field and the temperature on the surfaces the CFD solution with connecting mesh was used. Absorption coefficients was generated with HITRAN and HITEMP [34, 35]. The sensor was placed 1km from the aircraft and the atmospheric moderation was estimated by using MODTRAN [36] with the subarctic-summer model. No background was considered.

The elevation angles reached from -30° to 10° in steps of 5° and for each elevation angle the azimuth angle reached from 0° to 180°, due to symmetry, in steps of 5°. This gave a total of 333 calculation cases.

In Figure 6.4, some radiance images are presented and in Figure 6.5, polar plots for an angle of -5° are presented. The scales are different in the two images in Figure 6.5.

The result shows that the use of a material with the emissivity equals to 0.7 is insufficient [37]. Angle dependent signature paint with very low emissivity can be applied. This treatment decreases the signature drastically. However, treatment with low emissivity paint will also increase the reflectivity, which is defined as one minus the emissivity, of objects. Thus, reflections from the ground, the sky and the sun will increase. This treatment was done in the project "Design of a Low Signature UCAV" and the complete analysis from both projects are presented in Ref. [37].

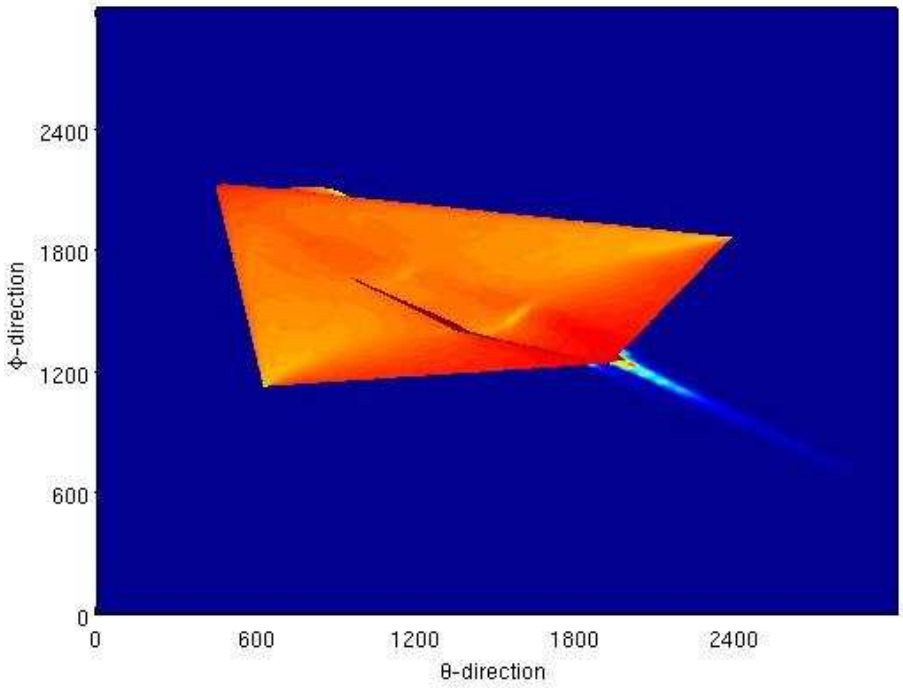


(a) Azimuth: 40°, Elevation: -30°, 3-5$\mu$m

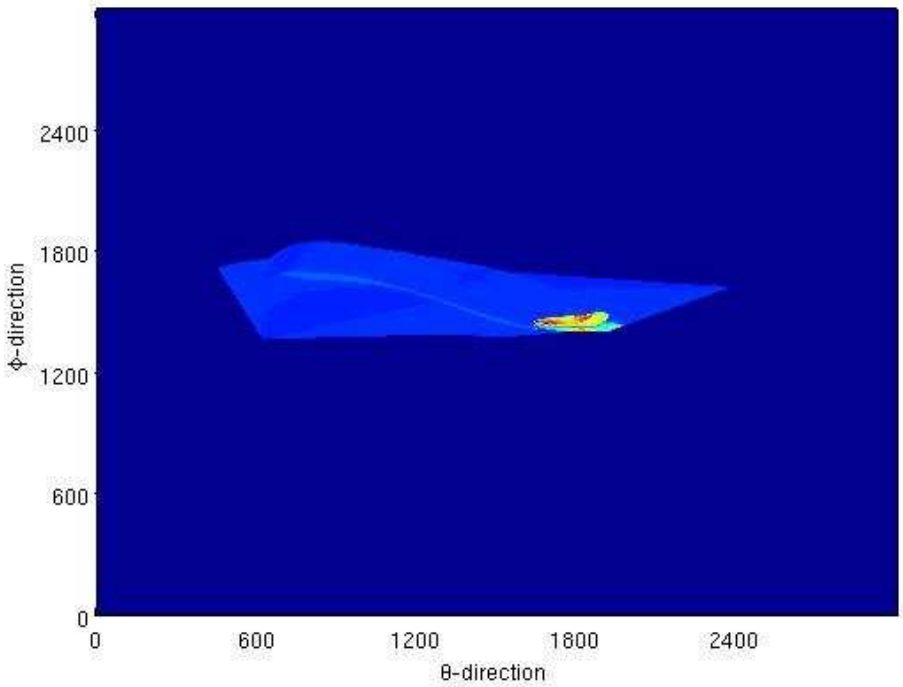


(b) Azimuth: 140°, Elevation: 10°, 8-12$\mu$m

Figure 6.4: Radians images.

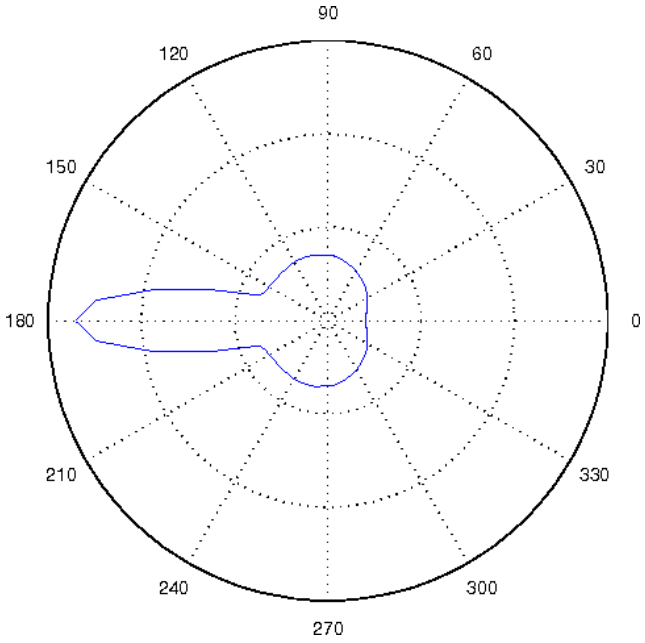


(a) 3-5$\mu$m, without treatment

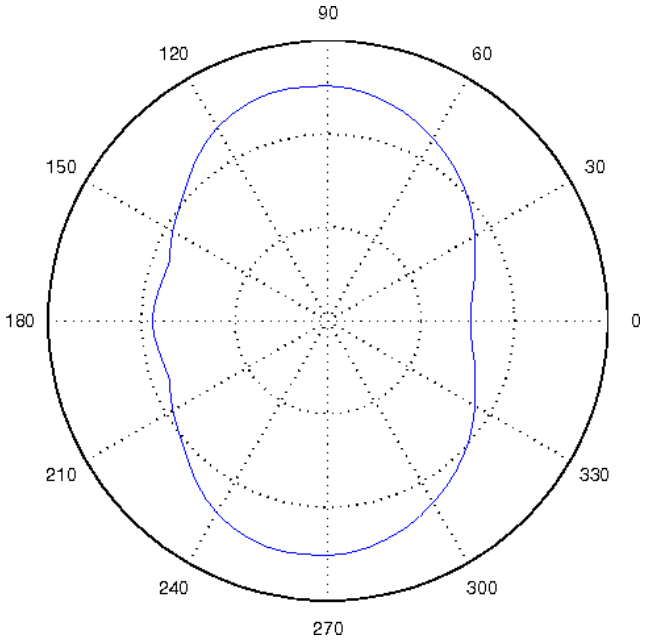


(b) 8-12$\mu$m, without treatment

Figure 6.5: Polar plots of the total intensity for the EIKON, at elevation angle -5° for wavelength interval 3-5$\mu$m (left) and interval 8-12$\mu$m (right).

# 7 Propulsion systems

A general competence in the field of vehicle propulsion was being developed by studying different engine concepts and development trends. The working principles, integration/design issues, operational properties, advantages and drawbacks of the concepts are addressed and documented. The work was carried out in collaboration with other projects within FoT25, and the knowledge on propulsion serve as a resource for these projects. Having studied these issues, a proper choice of the propulsion system for a particular vehicle was enabled.

Depending on a number of mission requirements on the vehicle, such as, distance flown with a military load, manoeuvre capability, dash, loitering, and stealth properties, the propulsion system is chosen. These requirements and the size of the vehicle determine the type and thrust level of the propulsion system.

Engine concepts are either based on single- or multi cycles (e.g. PDE - Ramjet). The well-known turbojet/turbofan technology and the novel concepts PDE and ATR are the more promising for vehicle propulsion. All are based on the Brayton cycle (heat addition at constant pressure), except the PDE engine which is based on the more efficient Humphrey cycle (heat addition at constant volume) [1].

For the purpose of a conceptual UAV studied within the FoT25-project "Conceptual design studies", a turbofan engine with afterburner has been designed [2]. Off-design performance data for the flight envelope have been obtained.

# 8 Reports and publications

## General

Marlene Andersson, Ola Hamnér, Rolf Jarlås och Staffan Meijer: "Flygteknikstudier för det nya seklet", Flygteknik 2004, Flygtekniska föreningen, 2004.

Marlene Johansson: "Propulsion Integration in an UAV", AIAA-2006-2834, 2006. *Presented at 24th AIAA Applied Aerodynamics Conference, San Francisco, USA, 5-8 June 2006.*

Marlene Johansson: "Propulsion Integration in an UAV". *Presented at Joint EWA and DESider Workshop on Validation of Numerical Methods by Experiments in Aerodynamics, Linköping/Stockholm, 13-14 June 2006.*

Marlene Johansson (editor): "FoT25 2003-2005: Propulsion Integration - Final Report", FOI-R--2017--SE, 2006.

## Aerodynamics

Adam Jirásek: "A Modified Vortex Generator Model and its Application to Complex Aerodynamic Flows", FOI-R--1204--SE, 2004.

Adam Jirásek: "A Vortex Generator Model and its Application to Flow control", Journal of Aircraft, vol. 6, no. 42, 2005.

Magnus Tormalm, Adam Jirásek och Marlene Andersson: "Design och CFD-beräkningar av smyganpassade luftintag inklusive intagskanaler och virvelgeneratorer", FOI-MEMO-1417, 2005.

Ingemar Samuelsson: "Test of an UCAV (Eikon) Air Inlet Duct at Static Conditions in FOI S1 Suckdown Facility", FOI-R--1572--SE, 2005.

Adam Jirásek: "Development and Application of Design Strategy for Design of Vortex Generator Flow Control in Inlets", AIAA-2006-1050, 2006.

Magnus Tormalm: "Design and Analysis of Compact UAV Ducts", AIAA-2006-2828, 2006. *Presented at 24th AIAA Applied Aerodynamics Conference, San Francisco, USA, 5-8 June 2006.*

Adam Jirásek: "Final report on VG flow control in FOI-EIC-01 inlet", FOI-RH--0553--SE, 2006.

Magnus Tormalm: "Propulsion Integration Project, Design and analysis of compact UAV ducts", FOI-R--2019--SE, 2006.

Dag Eriksson and Ingemar Samuelsson: "A Note on the Control of Corrected Mass Flow Rate at Wind Tunnel Tests of Air Inlet Models", FOI report in manuscript, 2006.

Ingemar Samuelsson: "Test of Effect of Vortex Generators in the Diffuser Duct of an UCAV Air Inlet (Forebody Model of Eikon) in FOI Transonic Wind Tunnel T1500", FOI report in manuscript, 2006.

## Material and structure dynamics

Mats Dalenbring and Niklas Sehlstedt:"Propulsion Integration - Material Technology (Status Report)", FOI-Memo-1199, 2005.

Mats Dalenbring and Adam Zdunek: "On the use of three-dimensional h- and p-version finite elements in solving vibration response problems", Journal of Sound and Vibration, Volume 288, Issues 4-5, Pages 907-929, 2005.

Mats Dalenbring and Jonathan Smith: "Simulation of S-Duct Dynamics using Fluid-Structure Coupled CFD", AIAA-2006-2981, 2006. *Presented at 24th AIAA Applied Aerodynamics Conference, San Francisco, USA, 5-8 June 2006.*

Jonathan Smith and Mats Dalenbring: "Aeroelastic Simulation of S-Duct Dynamics using Fluid-Structure Coupled CFD", Proc. 26th Congress of the International Council of the Aeronautical Sciences (ICAS), September 2006, In manuscript.

Mats Dalenbring: "Analysis of Material and Structures used within the FoT25 Project Propulsion Integration", FOI-R--2024--SE, 2006.

## Stealth technology

Niklas Sehlstedt and Adam Zdunek: "Influence to cavity RCS by curvature, RAM and vortex generators", FOI-R--1531--SE, 2005.

Ulf Tengzelius and Niklas Sehlstedt: "Results of RCS calculations on Eikon no 6 outlet cavity", FOI-RH--0505--SE, 2005.

Niklas Sehlstedt, Ulf Tengzelius and Marlene Johansson: "Results of RCS calculations on an UCAV inlet cavity", FOI-RH--0532--SE, 2005.

Marlene Johansson and Mats Dalenbring: "SIGGE, a prediction tool for aeronautical IR signatures, and its applications", AIAA-2006-3276, 2006.*Presented at 9th AIAA/ASME Joint Thermophysics and Heat Transfer Conference, San Francisco, USA, 5-8 June 2006.*

Marlene Johansson: "AP3.5 Koppling TVC-IR", FOI Memo 1720, 2006.

Mats Dalenbring och Marlene Johansson, "FoT25 - IR calculations of Eikon within the projects Design of a Low Signature UCAV and Propulsion Integration", FOI-RH--0550--SE, 2006.

## Propulsion systems

Anders Hasselrot and Björn Montgomerie: "An Overview of Propulsion Systems for Flying Vehicles", FOI-R--1563--SE, 2005.

Björn Montgomerie: "Design of a Turbofan Engine Cycle with Afterburner for a Conceptual UAV", FOI-R--1835--SE, 2005.

# 9 Conclusions

A propulsion system has been designed for an UAV. FOI have had the main responsibility for the inlet including the duct. The flow in the duct has been optimized using vortex generators. Both the duct and the inlet including the duct have been tested in wind tunels as well as analyzed using CFD. The requirements for pressure recovery and distortion was achieved using vortex generators.

The inlet duct and the outlet have been analyzed using fluid-structure dynamics and RCS calculations. The outlet, designed by Volvo Aero, has been analyzed using RCS- and IR calculations.

Different propulsion systems has been studied and an engine has been designed for a conceptual UAV.

# Bibliography

[1] A. Hasselrot and B. Montgomerie. An overview of propulsion systems for flying vehicles. FOI-R–1563–SE, 2005.

[2] B. Montgomerie. Design of a turbofan engine cycke with afterburner for a conceptual uav. FOI-R–1835–SE, November 2005.

[3] A. Zdunek and W. Rachowicz. A goal-oriented hp-adaptive finite element approach to radar scattering problems. *Computer Methods in Applied Mechanics and Engineering*, 194, 2005.

[4] A. Zdunek, W. Rachowicz, and N. Sehlstedt. Toward hp-adaptive solution of 3D electromagnetic scattering from cavities. *Computers and Mathematics with Application*, 49, 2005.

[5] W. Rachowicz and A. Zdunek. An hp-adaptive finite element method for scattering problems in computational electromagnetics. *International Journal for Numerical Methods in Engineering*, 62, 2005.

[6] M. Johansson and M. Dalenbring. Calculation of IR signatures from airborne vehicles. *SPIE paper 6228-40*, 2006.

[7] M. Johansson and M. Dalenbring. SIGGE, a prediction tool for aeronautical IR signatures, and its applications. *AIAA-2006-3276*, 2006.

[8] A. Jirásek. Vortex-Generator Model and its Application to Flow Control. *Journal of Aircraft*, 6(42), 2005.

[9] A. Jirásek. Development and Application of Design strategy for Design of Vortex Generator Flow Control in S-ducts. *AIAA-2006-1050*, 2006.

[10] M. Andersson, O. Hamnér, R. Jarlås, and S. Meijer. Flygteknikstudier för det nya seklet. Flygteknik 2004, Flygtekniska föreningen, 2004.

[11] S. Meijer. The FoT25 2003-2005 project Design of a Low Signature UCAV Final report. FOI report in manuscript, 2006.

[12] R. Avellan. FoT25 TVC/LO Intag och Utlopp - Kravspecifikation för luftintag, utloppsmunstycke och TVC. 2004VAC001985, Företagshemlig, 2004.

[13] A. Lundbladh. Motorval EIKON för TVC/LO. 2004VAC003126, utg. 1, Företagshemlig, 2004.

[14] Edge flow solver, http://ww.foi.se/edge.

[15] P. Eliasson. EDGE, a Navier-Stokes solver for unstructured grids. In *Proc. to Finite Volumes for Complex Applications III*, pages 527–534. ISBN 1 9039 9634 1, 2002.

[16] B. Andersson, U. Falk, I. Babuska, and T. von Petersdorff. Reliable Stress and Fracture Mechanics Analysis of Complex Components Using a h-p Version of FEM. *International Journal for Numerical Methods in Engineering*, 38, 1995.

[17] M. Dalenbring and A. Zdunek. On the use of three-dimensional h- and p-version finite elements in solving vibration response problems. *Journal of Sound and Vibration*, 288, 2005.

[18] M. Johansson and M. Dalenbring. SIGGE v.2.3.1 - Users Guide. FOI-R–2018–SE, 2006.

[19] M. Tormalm. Propulsion Integration Project - Design and analysis of a compact UAV duct. FOI-R–2019–SE, 2006.

[20] M. Tormalm. Design and Analysis of Compact UAV Ducts. *AIAA-2006-2828*, 2006.

[21] I. Samuelsson. Test of an UCAV (Eikon) Air Inlet at Static Condition in FOI S1 Suckdown Facility. FOI-R–1572–SE, 2005.

[22] I. Samuelsson. Test of Effect of Vortex Generators in the Diffuser Duct of an UCAV Air Inlet (Forebody Model of Eikon) in FOI Transonic Wind Tunnel T1500. FOI report in manuscript, 2006.

[23] B. H. Anderson and J. Gibb. Vortex Generator Installation of Steady State and Dynamic Distortion. *AIAA-1996-3279*, 1996.

[24] B. G. Allan, L. R. Owens, and J. C. Lin. Optimal Design of Passive Flow Control for a Boundary-Layer-Ingesting Offsert Inlet Using Desing-of-Experiments. *AIAA-2006-1049*, 2006.

[25] A. Jirásek. Final report on VG Flow control in FOI-EIC-01 inlet. FOI-RH–0553–SE, 2006.

[26] B. Gustafsson. FoT25 nyckelteknologiprojektet TVC/LO Intag och Utlopp - AP 2.5 Analys CFD. 2005VAC001418, Företagshemlig, 2005.

[27] M. Dalenbring. Analysis of Material and Structure used within the FoT25 Project Propulsion Integration. FOI-R–2024–SE, 2006.

[28] M. Dalenbring and J. Smith. Simulation of S-Duct Dynamics using Fluid-Strucutred Coupled CFD. *AIAA-2006-2981*, 2006.

[29] J. Smith and M. Dalenbring. Aeroelastic Simulation of S-Duct Dynamics using Fluid-Strucutred Coupled CFD. *Proc. 26th Congress of the International Council of the Aeronautical Sciences*, September 2006. In manuscript.

[30] J. Smith. Aeroelastic fucntionality in Edge, Initial implementation and validation. FOI-R–1485–SE, 2005.

[31] N. Sehlstedt, U. Tengzelius, and M. Johansson. Results of RCS calculations on an UAV inlet cavity. FOI-RH–0532–SE, 2005.

[32] U. Tengzelius and N. Sehlstedt. Results of RCS calculation on Eikon no 6 outlet cavity. FOI-RH–0505–SE, 2005.

[33] N. Sehlstedt and A. Zdunek. Influence to cavity RCS by curvature, RAM and vortex generators. FOI-R–1531–SE, 2005.

[34] L. Rothman. The Hitran Molecular Spectroscopic Database and Hawks (Hitran Atmospheric Workstation): 1996 edition. *Journal of Quantitative Spectroscopy and Radiative Transfer*, 60, 1998.

[35] *The HITRAN Database*, http://www.hitran.com.

[36] *MODTRAN*, http://www.ontar.com.

[37] M. Dalenbring and M. Johansson. FoT25 - IR calculations of Eikon within the projects "Design of a Low Signature UCAV" and "Propulsion Integration". FOI-RH–0550–SE, 2006.